Available online at www.sciencedirect.com
ScienceDirect
Journal of the European Ceramic Society 31 (2011) 1199–1210
www.elsevier.com/locate/jeurceramsoc

Crack propagation and stress distribution in binary and ternary directionally solidified eutectic ceramics

L. Perrière [a,b], R. Valle [a,*], N. Carrère [a], G. Gouadec [c], Ph. Colomban [c], S. Lartigue-Korinek [b], L. Mazerolles [b], M. Parlier [a]

[a] *ONERA/DMSC, 29 avenue de la Division Leclerc, F-92322 Châtillon, France*
[b] *ICMPE, UMR 7182, CNRS–Univ. Paris Est, 2-8 rue H. Dunant, F-94320 Thiais, France*
[c] *LADIR, UMR 7075, CNRS–Univ. P. et M. Curie (Paris 6), 2-8 rue H. Dunant, F-94320 Thiais, France*

Abstract

The development of directionally solidified eutectic (DSE) ceramics for gas turbine applications necessitates improving their strength and toughness. The early stage of crack propagation is investigated in either binary ($Al_2O_3/Y_3Al_5O_{12}$, $Al_2O_3/GdAlO_3$ and $Al_2O_3/Er_3Al_5O_{12}$) or ternary ($Al_2O_3/Y_3Al_5O_{12}/ZrO_2$, $Al_2O_3/GdAlO_3/ZrO_2$ and $Al_2O_3/Er_3Al_5O_{12}/ZrO_2$) DSE ceramics. *Post-mortem* scanning electron microscopy (SEM) examination of biaxial flexure induced cracks revealed crack deflection and branching in the various phases and in the phase boundaries. These observations are correlated to analytical and finite element (FE) internal stress calculations, FE determination of the axial shear stress component in the interfaces in the vicinity of the specimen surface (free-edge effect) and FE calculations of the stress distribution resulting from an applied loading. Results from ruby (Cr^{3+}) fluorescence piezo-spectroscopy measurements are analyzed, taking into account the hydrostatic and plane stress hypotheses. Moreover, transmission electron microscopy (TEM) examinations have confirmed the role of interfaces in the crack nucleation and propagation modes.

Keywords: Eutectic ceramics: Composites; Al_2O_3; Fracture; Residual stresses

1. Introduction

The development of new ultra high temperature structural materials in the aerospace field and in particular for gas turbine applications is a real challenge. Despite the various studies performed to increase the heat-resistance of nickel-based superalloys, their use at temperatures beyond 1400 K remains difficult. For higher temperatures, sintered ceramic oxides offer many advantages compared to superalloys: resistance to oxidation and abrasion, lower density. Unfortunately, sintered ceramics are brittle and their failure strength decreases when the temperature increases. Ceramic materials prepared from oxides by unidirectional solidification from the melt (melt growth composites (MGC)) add new potentialities to the advantages of sintered ceramics: a higher strength, almost constant up to temperatures close to the melting point (no amorphous phases at the interfaces), good creep resistance, stability of the microstructure and no chemical reaction between the constituent phases.[1–3] The microstructure of directionally solidified eutectic (DSE) ceramics consists in three-dimensional (3-D) and continuous interconnected networks of single-crystal eutectic phases. After solidification of binary eutectics, the eutectic phases are alumina and either an $LnAlO_3$ perovskite phase (Ln, lanthanide element: Gd, Eu) or an $Ln_3Al_5O_{12}$ garnet phase (Ln: Y, Yb, Er, Dy). In the case of ternary systems, zirconia is added as a third phase in order to refine the microstructure and to promote energy dispersive crack deflection modes acting in favour of a better toughness. In the present case, the directionally solidified eutectic ceramics under investigation are either binary ($Al_2O_3/Y_3Al_5O_{12}$ (YAG), $Al_2O_3/Er_3Al_5O_{12}$ (EAG) and $Al_2O_3/GdAlO_3$ (GAP)) or ternary (Al_2O_3/YAG/ZrO_2, Al_2O_3/EAG/ZrO_2 and Al_2O_3/GAP/ZrO_2) eutectics. Studies to control the microstructure of directionally solidified eutectic ceramics have been performed, acting on the processing parameters of the floating-zone method (arc image furnace).[4–8] The mechanical properties have thus been investigated on the small specimens manufactured through this

* Corresponding author. Tel.: +33 1 46 73 45 69; fax: +33 1 46 73 41 42.
E-mail address: roger.valle@onera.fr (R. Valle).

0955-2219/$ – see front matter © 2010 Elsevier Ltd. All rights reserved.
doi:10.1016/j.jeurceramsoc.2010.09.016

process. A biaxial testing disc flexure device[9] has been used to investigate the early stage of crack propagation in the interconnected microstructure of the DSE ceramics. *Post-mortem* scanning electron microscopy (SEM) examination of the biaxial flexure induced cracks is focused on the possibility of crack deflection in the various phases and in the phase boundaries, a phenomenon which may markedly improve the toughness of these eutectic composites. However, the mechanical properties and the crack propagation modes depend on the level of the internal thermal stresses. In this context, internal stresses measurements have already been performed in eutectic ceramics using either X-ray[10,11] or neutron[12] diffraction techniques or fluorescence piezo-spectroscopy.[3,13–15] Analytical and finite element (FE) calculations of the thermal mismatch stresses can also be performed; they however require the prior knowledge of the thermomechanical parameters of the various phases[16–24] and of the eutectic composites.[25]

Consequently, complementary measurements have been performed, not only on the eutectic composites, but also on the individual garnet and perovskite phases. Even if analytical calculations had already provided a good estimate of the residual stress level in the vicinity of the interfaces in the simple configuration of infinite concentric cylinders,[9] additional FE stress calculations have been performed in order to map the stress components in more complex geometrical configurations. Moreover, concerning the free-edge effect in the vicinity of the specimen surface, FE calculations have permitted to determine the axial shear stress component in the interfaces. Internal stress measurements through ruby (Cr^{3+}) fluorescence piezo-spectroscopy have provided an average value of the stress state in the alumina phase of the various investigated DSE composites. The fluorescence signal being emitted from a small depth interaction volume, FE calculations, taking into account the presence of the neighbouring surface, have allowed comparing these experimental results with those of analytical and FE calculations representative of the bulk material. Furthermore, transmission electron microscopy (TEM) examinations were performed in order to investigate, at a finer scale, the role of the interfaces in crack nucleation and propagation. Finally, a comparative analysis of all these complementary experimental and calculated results was aimed at a better understanding of the role of the interfaces in the fracture modes and on the toughness of the DSE composites.

2. Experimental procedures

2.1. Materials

Eutectic samples are prepared from high purity powders (Al_2O_3: Baikowski Chimie, France; Y_2O_3, Er_2O_3, Gd_2O_3: Rhodia, formerly Rhône Poulenc, France; ZrO_2: Th. Goldschmidt Industriechemikalien, Germany) mixed at the ratios corresponding to the eutectic compositions.[4,26–30] Rods, isostatically pressed at room temperature, are then sintered at 1675 K for 10 h in order to improve their handling strength. Directional solidification is performed in air using the floating-zone translation technique (6 kW xenon lamp arc image furnace) at a solidification rate of 10 mm h^{-1}, or 20 mm h^{-1} in the only case of Al_2O_3/EAG/ZrO_2. Final rods of oriented eutectics are about 6–8 mm in diameter and 40–60 mm in length.

2.2. Biaxial flexure testing

Biaxial flexure testing was preferred to beam-bending tests since the coaxial-ring test is free of edge condition influences[31]: cracks initiate in the central area and propagate outwardly. On the contrary, the beam-bending test is influenced markedly by the edges parallel to the specimen major axis, the presence of flaws leading to premature and non-representative crack initiation. The biaxial disc flexure testing device[9] presents the ring supported/ring loaded test geometry (Fig. 1). The stress components may thus be determined through an analytical calculation.[32] In the central area (Fig. 1), inside the inner loading ring ($0 \le r \le r_0$), the radial (σ_r) and tangential (σ_θ) stress components are equal, uniform and maximum. The main advantage of this system, as concerns the initiation of cracks and the early stage of crack propagation, is thus the possibility to subject the relatively large central area, which is free from edge defects, to a uniform biaxial tensile loading.

Specimens for the biaxial bending tests (≈800 μm in thickness) are cut perpendicularly to the growth axis of the 8 mm in diameter eutectic rods, the 5 mm in diameter discs being then cut in the central area of the slice. High quality surface finish of the lower surface of the specimen (i.e. the surface which will be subjected to the biaxial tensile loading), is obtained through diamond polishing. The biaxial bending tests are conducted at room temperature. After the flexure tests, examination of cracks is performed through scanning electron microscopy (SEM): Zeiss Gemini (field emission gun (FEG)-SEM).

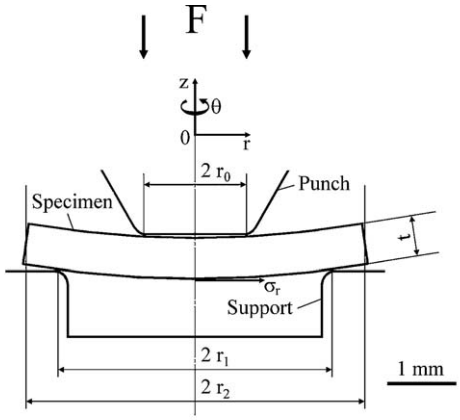

$$\sigma_r(r \le r_0, \theta) = \sigma_\theta(r \le r_0, \theta) = \frac{3(1+\nu)F}{4\pi t^2}\left[2\ln\frac{r_1}{r_0} + \frac{1-\nu}{1+\nu}\frac{r_1^2 - r_0^2}{r_1^2}\frac{r_1^2}{r_2^2}\right]$$

Fig. 1. Biaxial disc flexure test: the specimen under biaxial loading between the flat-ended punch (radius r_0) and the support (radius r_1), with specimen overhang (r_2–r_1). In the central area, the radial (σ_r) and tangential (σ_θ) stress components are equal, uniform and maximum (F: applied force, ν: Poisson's ratio of the specimen, t: specimen thickness).[9]

2.3. Thermomechanical testing

Dilatometric measurements in the longitudinal direction are performed in an Adamel (DI24) thermoanalyser. Rods, approximately 8 mm in diameter and 15 mm in length, are used for these measurements, the sample ends being ground flat and parallel.

In order to perform dilatometric measurements on the isolated garnet or perovskite phases, polycrystalline rods of YAG, EAG and GAP are prepared using the same oxide powders mixed at the ratios corresponding to the composition of YAG ($Y_3Al_5O_{12}$), EAG ($Er_3Al_5O_{12}$) and GAP ($GdAlO_3$) phases, respectively.[26–28] After being isostatically pressed at room temperature, the rods are sintered at 1975 K for 48 h. The single phase nature of the polycrystalline rods thus obtained is verified through X-ray diffraction.[5] Although the lanthanide oxide (Y_2O_3, Er_2O_3 or Gd_2O_3) molar content of the zirconia phase in the eutectics is rather high (≈20 mol%),[4] dilatometric measurements have been performed on commercially available ZrO_2 sintered rods (stabilized cubic ZrO_2–8.2 mol% Y_2O_3: Kyocera, Japan).

Measurement of the longitudinal Young's modulus is performed through longitudinal compression tests. The parallelepipedal specimens, approximately 7 × 4 × 4 mm, are cut parallel to the solidification direction, using a diamond edged blade. These specimens are equipped with strain gauges mounted on two parallel sides. The tests are conducted on an electromechanical MTS (DY 37) testing system in the elastic domain. The brittle ceramic specimens are isolated from the compression plates by ductile aluminium foils. Taking advantage of the plastic deformation of the aluminium foils which progressively ensures a uniform applied loading on the two ends, the cyclic compressive stress level is increased by steps until the responses given by the two strain gauges become identical.[5] Unfortunately, the resulting mechanical cycling may sometimes lead to brittle failure of the specimen, thus impeding the experimental determination of the Young's modulus of the eutectic composite (e.g. Al_2O_3/EAG/ZrO_2 ternary DSE).

2.4. Micrometer scale fluorescence piezo-spectroscopy measurements of the internal stresses

Ruby fluorescence is used to determine the thermal residual stress level in the alumina phase of the binary and ternary eutectics (Cr^{3+} impurities generate sharp stress sensitive R_1 and R_2 fluorescence bands).[33,34] Fluorescence spectra are recorded using either a "XY" model Raman micro-spectrometer (Horiba-JY, formerly Dilor, France) equipped with a double monochromator as a filter and a back-illuminated liquid nitrogen cooled 2000 × 800 pixels CCD detector (Spex, Jobin-Yvon, France) or, in the only case of Al_2O_3/EAG/ZrO_2, a Labram HR Raman microspectrometer (Horiba-JY). The laser excitation (λ = 514.529 nm) is focused on Al_2O_3 phases through a 100× microscope objective (≈1 μm in diameter probe size) and the backscattered light analyzed. The motorized XY-stage (0.1 μm step) allows a very precise choice of the analyzed area.[35,36] Five to 30 spectra are recorded in each eutectic composite and emission lines from a neon lamp are used to control the spectrometer calibration.

2.5. Microstructural investigations

Growth directions, orientation relationships between eutectic phases and structure of interfaces are investigated by transmission electron microscopy (TEM). These observations are performed on thin foils of transverse sections using either a conventional TEM (JEOL 2000EX) or a high-resolution TEM (Topcon 002B), both operating at 200 kV.

3. Results

3.1. Crack propagation modes

The essential propagation mode in the six investigated directionally solidified eutectics is transgranular crack propagation.[9] Following the zig–zag propagation of a crack over a long distance in the Al_2O_3/YAG binary eutectic composite confirms these previous observations (Fig. 2a). This type of crack propagation does not only result from deflections of the cleavage crack inside each phase or when crossing phase boundaries, but also from crack deflection in these interfaces themselves. The interfaces may thus play a major role in the nucleation and propagation of cracks. In both binary[9] and ternary eutectics, interface crack propagation is observed between Al_2O_3 and YAG (large black arrows in Fig. 2a and b), Al_2O_3 and EAG (large black arrows in Fig. 2c), Al_2O_3 and GAP (large black arrows in Fig. 2d), Al_2O_3 and ZrO_2 (white arrows in Fig. 2b–e), YAG and ZrO_2 (sharp black arrow in Fig. 2b), EAG and ZrO_2 (sharp black arrow in Fig. 2c) and GAP and ZrO_2 (sharp black arrow in Fig. 2d). Crack branching is also observed (split arrows in Fig. 2a, b and e), although, in most cases, these bifurcation mechanisms lead to stopped cracks.

3.2. Thermomechanical behaviour

The coefficients of thermal expansion (CTE) of Al_2O_3 single crystals (directions // and ⊥ **c**), of the isolated YAG ($Y_3Al_5O_{12}$), EAG ($Er_3Al_5O_{12}$), GAP ($GdAlO_3$) and ZrO_2 phases and of the investigated binary and ternary eutectic ceramics (longitudinal direction) are reported in Table 1. The CTEs found for Al_2O_3 are in good agreement with those found in the literature and confirm the quality of calibration of the thermoanalyser. These experimentally determined values will be used for the internal stress calculations. Concerning the DSE ceramics, it should be noted that the CTEs of the three ternary eutectics are higher than those of the corresponding binary eutectics. In each case, the percentage of lanthanide oxide (Y_2O_3, Er_2O_3 or Gd_2O_3) addition in the zirconia phase is high (≈20 mol%),[4] much higher than that of the zirconia specimen used for the CTEs measurements. However, the CTEs measured on the stabilized cubic ZrO_2–8.2 mol% Y_2O_3 are rather high and in good agreement with those found in the literature.[16–19] The higher values of the CTEs of the ternary eutectics, as compared with the binary eutectics, may thus be explained by the high value of the CTEs of the zirconia phases, fully stabilized cubic ZrO_2 with Y_2O_3, Er_2O_3 or Gd_2O_3 additions.

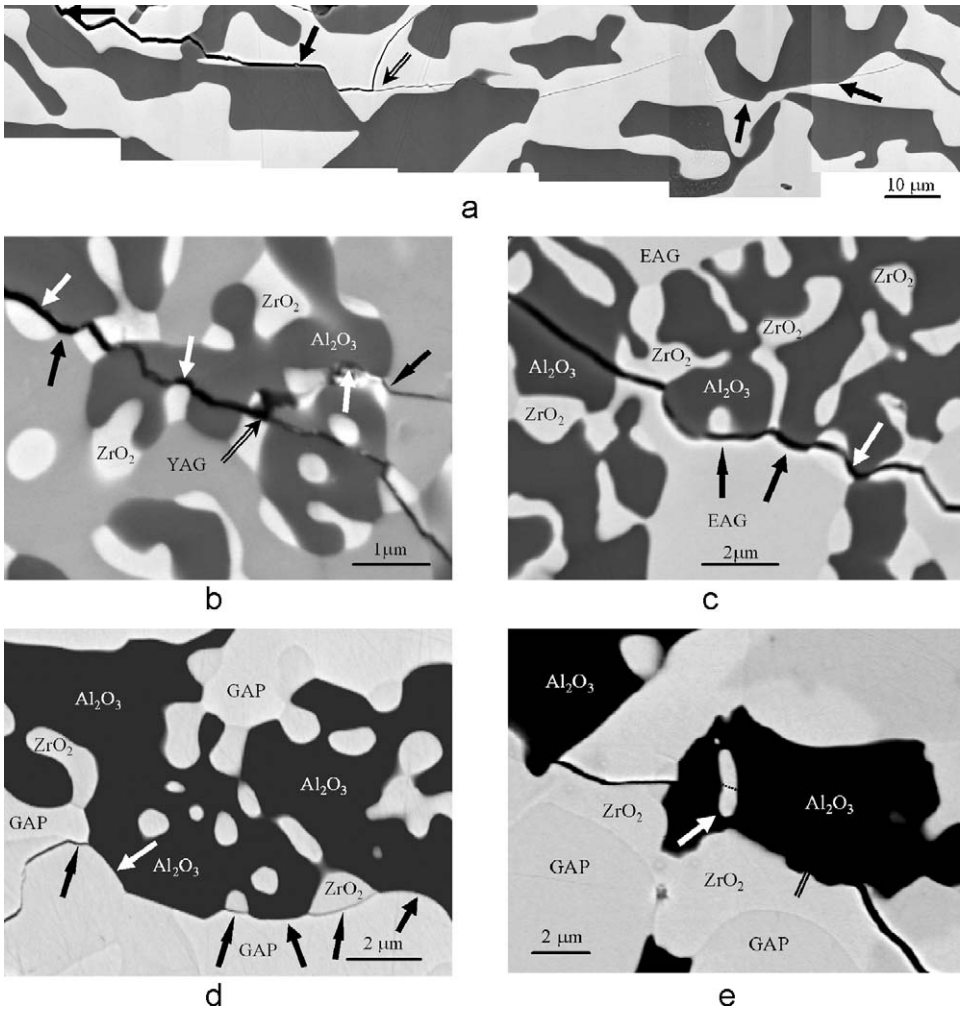

Fig. 2. Crack propagation modes at room temperature in eutectic ceramics subjected to biaxial flexure (FEG-SEM, back-scattered electrons): Al_2O_3/YAG (a), Al_2O_3/YAG/ZrO_2 (b), Al_2O_3/EAG/ZrO_2 (c) and Al_2O_3/GAP/ZrO_2 (d and e).

Table 1
Coefficients of thermal expansion (CTEs) of Al_2O_3 single crystals (directions // and ⊥ **c**), of the YAG, EAG and GAP polycrystalline samples, of commercial sintered ZrO_2 (8.2 mol% Y_2O_3) and of the investigated eutectic ceramics (longitudinal direction) (*: 1400 K).

System	α (10^{-6} K^{-1}) 500 K	α (10^{-6} K^{-1}) 1000 K	α (10^{-6} K^{-1}) 1500 K
Al_2O_3 // c	8.2	9.3	10.5
Al_2O_3 ⊥ c	8	8.7	9.5
YAG	7.8	8.8	9.7
EAG	8.2	9.0	9.8
GAP	6.4	7.7	8.8*
ZrO_2 (8.2 mol% Y_2O_3)	9.0	9.6	10.4
Al_2O_3/YAG	8.3	9.1	9.9
Al_2O_3/YAG/ZrO_2	8.4	9.2	10.1
Al_2O_3/EAG	8.2	9	9.3
Al_2O_3/EAG/ZrO_2	8.2	9.3	10.3
Al_2O_3/GAP	8.1	9.1	10
Al_2O_3/GAP/ZrO_2	8.1	9.5	10.9

Concerning the determination of the Young's moduli of the various eutectic composites through compression tests, the results of these measurements are reported in Table 2. The eutectic ceramics being two- or three-phase composites, the measured average moduli may be compared to those determined using either the Voigt (uniform strain) or Reuss (uniform stress) methods. The Voigt modulus (E_{Voigt}) thus corresponds to the rule of mixture (ROM) modulus in the longitudinal direction of a unidirectional composite, whereas the Reuss modulus (E_{Reuss}) corresponds to the ROM modulus in the transverse direction of

Table 2
Young's moduli of the various eutectic composites determined through compression tests.

System	E (GPa)
Al_2O_3/YAG	326
Al_2O_3/YAG/ZrO_2	333
Al_2O_3/EAG	320
Al_2O_3/GAP	310
Al_2O_3/GAP/ZrO_2	300

a unidirectional composite.

$$E_{\text{Voigt}} = V_1 E_1 + V_2 E_2 \quad (1)$$

$$\frac{1}{E_{\text{Reuss}}} = \frac{V_1}{E_1} + \frac{V_2}{E_2} \quad (2)$$

where V_1 and V_2 are respectively the volume fractions of phases 1 and 2.

The Voigt and Reuss moduli may thus be determined using the values found in the literature[20–23] for the Young's moduli of the individual phases (Al_2O_3, YAG, ZrO_2) and the volume fractions experimentally determined through image analysis.[4] In this respect, the measured Young's modulus (326 GPa) for the Al_2O_3/YAG eutectic ($V_{Al_2O_3} = V_{YAG} = 50\%$) is closer to that given by the Reuss modulus (339 GPa) than to that given by the Voigt modulus (355 GPa). The mechanical behaviour in the elastic domain (Young's modulus) of the 3-D interconnected eutectic composite is thus essentially governed by the portion of phases elongated in the transverse direction (ROM modulus in the transverse direction of a unidirectional composite). However, in the case of the Al_2O_3/YAG/ZrO_2 ternary eutectic ($V_{Al_2O_3} = 43\%$, $V_{YAG} = 43\%$, $V_{ZrO_2} = 14\%$), the measured Young's modulus (333 GPa) is located between the Reuss (321 GPa) and Voigt moduli (339 GPa), thus suggesting a complex mechanical behaviour in the elastic domain, influenced by both the longitudinal and transverse contributions of the various phases subjected to a uniaxial loading.

3.3. Internal stresses

The piezo-spectroscopic internal stress measurements in the alumina phase are performed using a micro-Raman spectrometer to detect chromium ion fluorescence. Cr^{3+} impurities are responsible for R_1 and R_2 stress sensitive fluorescence lines and the relationship between the frequency shift ($\Delta\nu$) in the spectrum and the state of stress of alumina is given by[33]

$$\Delta\nu = \Pi\,\sigma \quad (3)$$

where Π and σ are respectively the piezospectroscopic and stress tensors.

These tensors are defined in the ($\langle 1\,\bar{2}\,1\,0\rangle$, $\langle 1\,0\,\bar{1}\,0\rangle$, $\langle 0\,0\,0\,1\rangle$) orthogonal frame of α-$Al_2O_3$. The coefficients of the piezospectroscopic tensor have been determined experimentally in Cr^{3+}-doped sapphire.[34]

If a hydrostatic 3-D stress system (σ_{hydro}) is assumed, then the frequency shifts are given by[5,37]

$$\Delta\nu_{R_1} = 7.59\,\sigma^{R_1}_{\text{hydro}} \quad (4)$$

$$\Delta\nu_{R_2} = 7.61\,\sigma^{R_2}_{\text{hydro}} \quad (5)$$

where the units of frequency shift and stress are respectively cm^{-1} and GPa.

Concerning the crystallographic orientation of the alumina phase, electron backscattered diffraction (EBSD) and TEM investigations[4–7] have shown that the growth direction (i.e. the normal (z) to the specimen surface in the present measurements) is $\langle 1\,0\,\bar{1}\,0\rangle$ in all the binary and ternary DSEs under consideration. The other two axes of the orthogonal frame of the α-Al_2O_3 crystal, directions $\langle 0\,0\,0\,1\rangle$ and $\langle 1\,\bar{2}\,1\,0\rangle$, are thus parallel to the specimen surface (x, y plane). The fluorescence signal being emitted from a small depth interaction volume,[35] much smaller than the size of the interconnected microstructure of the eutectics, the stress state in the analyzed volume may be supposed to be essentially plane stress.[5,37] Consequently, the stress component in the direction normal to the polished surface is assumed to be zero ($\sigma_z = 0$) and the stress components in the plane perpendicular to this direction are supposed to be equal and given by $\sigma_x = \sigma_y = \sigma_{\text{planar}}$. Then[5,37]

$$\Delta\nu_{R_1} = 4.09\,\sigma^{R_1}_{\text{planar}} \quad (6)$$

$$\Delta\nu_{R_2} = 4.81\,\sigma^{R_2}_{\text{planar}} \quad (7)$$

The experimentally determined line shifts $\Delta\nu_{R_1}$ and $\Delta\nu_{R_2}$ may thus lead to different internal stress levels depending on the assumption of either a hydrostatic (σ_{hydro}) or plane stress (σ_{planar}) state. The hydrostatic (σ_{hydro}) and planar (σ_{planar}) internal stresses thus determined are reported in Table 3. It is worth noting that both the hydrostatic (σ_{hydro}) and planar (σ_{planar}) internal stresses in the alumina phase of the investigated eutectic composites are negative; the alumina phase is thus subjected to a compressive loading. It is also worth mentioning that the values obtained from the R_1 and R_2 lines shifts are similar in magnitude. As expected, the presence of the ZrO_2 phase in the ternary eutectics leads to higher values of the compressive stress. This phenomenon may be attributed to the high value of the coefficient of thermal expansion of the ZrO_2 phase as compared to those of the other phases.

4. Discussion

The various crack propagation modes observed using the biaxial bending tests have to be correlated to the level of the thermal mismatch stresses, to the stress distribution resulting from the applied loading and to the nature of the interfaces between the various phases.

4.1. Thermal mismatch stresses

Concerning the choice of a mechanical model representative of the 3-D interconnected microstructure, it should be noted that

Table 3
Chromium ion fluorescence-based internal stress measurements in the alumina phase of the binary and ternary eutectics. The experimental R_1 and R_2 peak positions were converted into equivalent stress values using hydrostatic (σ_{hydro}) or plane stress (σ_{planar}; $\sigma_z = 0$) models.

System	$\sigma^{R_1}_{\text{hydro}}$ (MPa)	$\sigma^{R_2}_{\text{hydro}}$ (MPa)	$\sigma^{R_1}_{\text{planar}}$ (MPa)	$\sigma^{R_2}_{\text{planar}}$ (MPa)
Al_2O_3–YAG	−90	−74	−166	−116
Al_2O_3–YAG–ZrO_2	−295	−255	−548	−403
Al_2O_3–EAG	−80	−67	−149	−106
Al_2O_3–EAG–ZrO_2	−401	−365	−743	−578
Al_2O_3–GAP	−208	−167	−386	−264
Al_2O_3–GAP–ZrO_2	−430	−363	−797	−574

the microstructure is essentially hieroglyphic in shape, instead of being fibrous or lamellar, as observed in regular eutectics.[38] In this context, the presence of a ZrO_2 phase totally embedded in Al_2O_3 (Fig. 3a (top center)) suggests the use of a model of concentric cylinders (Fig. 3b and c) to calculate the stress distribution. Contrary to the 1-D model of stacked plates, this 2-D model allows the determination of the normal stresses ($\sigma_n = \sigma_r$) acting on the interfaces between the various phases and resulting from this type of concentric arrangement.[9] For instance, the ZrO_2 phases in Fig. 3a (top center) may be represented by a 1 μm in diameter ZrO_2 bar, bonded into a 1.5 μm in thickness Al_2O_3 sleeve, surrounded by a 0.5 μm in thickness ZrO_2 sleeve (Fig. 3b and c). Finally, these three concentric cylinders are embedded into an equivalent homogeneous medium (EHM) having the diameter of the specimen under investigation and the macroscopic thermo-mechanical properties of the bulk Al_2O_3/GAP/ZrO_2 eutectics (Fig. 3b and c). Assuming linear elasticity, generalized plane strain and perfect bonding between the four concentric phases, a completely analytical solution is obtained.[39] In the case of the Al_2O_3/GAP/ZrO_2 eutectics subjected to a $\Delta T \approx 1700$ K temperature change, the normal stress (σ_r) acting on the ZrO_2/Al_2O_3 interface attains ≈1000 MPa[9]; this high tensile normal stress helps interface crack propagation, as observed in Fig. 3a. The external ZrO_2 layer is subjected to a high tensile circumferential loading ($\sigma_\theta \approx 1800$ MPa)[9] which helps transgranular crack propagation in this phase, as observed in Fig. 3a.

However, near the surface, another stress component has to be taken into consideration for the possibility of interface crack nucleation and propagation: the shear stress component τ_{rz} (Fig. 3c and d) which favours extrusion of the ZrO_2 phase subjected to a thermal compression loading. This shear stress component is zero on the surface (plane stress condition) and inside the specimen, far from the surface (plane strain condition). Close to the surface, due to free-edge effects, this shear stress component may attain a high value. An analytical approach of these effects being impossible, a fine mesh finite elements (FE) calculation, performed using the ZeBuLoN code,[40] is required to determine the maximum value. For instance, in the Al_2O_3/GAP/ZrO_2 eutectics, the shear stress component τ_{rz} attains 600 MPa at a distance of approximately 0.3 μm from the surface (Fig. 3b). In this region, the ZrO_2/Al_2O_3 interface is thus subjected to the combined effects of a high tensile normal stress ($\sigma_r \approx 1000$ MPa) and a high shear stress ($\tau_{rz} \approx 600$ MPa). Simultaneous relaxation of these two components of the thermal stresses explains the preferential crack nucleation and propagation in the Al_2O_3/ZrO_2 interface. It should be noted that, in the case of bending tests where the stress component resulting from

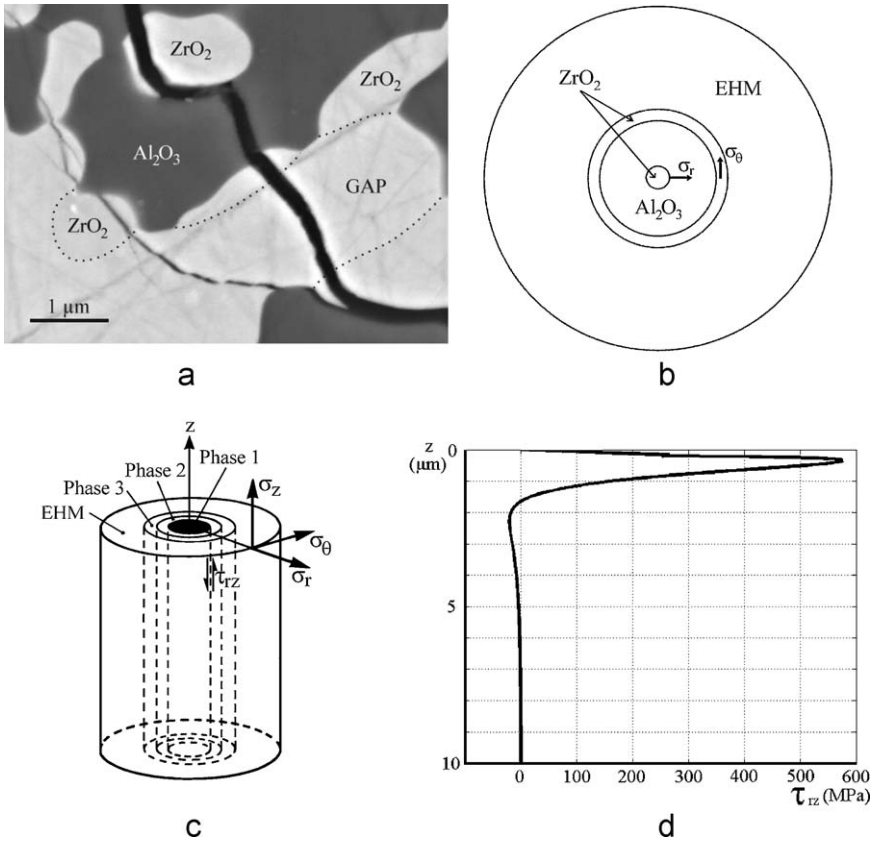

Fig. 3. Thermal mismatch stresses in the Al_2O_3/GAP/ZrO_2 eutectics. A ZrO_2 phase (top center) surrounded by a continuous layer of Al_2O_3 (a) and the corresponding model of concentric cylinders: ZrO_2 (phase 1), Al_2O_3 (phase 2), ZrO_2 (phase 3), embedded in an equivalent homogeneous medium EHM (b and c). Radial (σ_r), circumferential (σ_θ), axial (σ_z) and shear stress (τ_{rz}) components (c). Fine mesh FE calculation of the maximum value of the shear stress (τ_{rz}) in the Phase 1/Phase 2 cylindrical interface (d). This stress component which is zero on the surface (plane stress condition) and inside the specimen, far from the surface (plane strain condition), attains a very high value near the surface (d).

the applied loading is maximum on the surface, the combination of σ_r and τ_{rz} may lead to premature crack nucleation. This crack nucleation mode is not representative of the bulk material subjected to a tensile or compressive loading and may lead to lower values of the ultimate tensile strength when measured through bending tests. From a practical viewpoint, it should be noted that thermal cycling during service of a turbine blade may result in a to and fro displacement of the zirconia phase inside the alumina phase, thus leading to interface damage and finally to debonding.

Nevertheless, the model of concentric cylinders is only representative of this very simple geometrical configuration. Consequently, the stress component values thus determined can only be considered as estimates. The observed configurations are generally more complex and cannot be represented by a model of concentric cylinders. Examples are given in Fig. 2b (center), c (center), d (bottom) and e (center). In the first three cases, the ZrO_2 phase is not completely surrounded by the Al_2O_3 phase, whereas, in the last case (Fig. 2e), the ZrO_2 phase is elongated in one direction and broken. Representative models of these real geometrical arrangements are presented in Fig. 4a and b. The stress components can no more be determined through analytical calculations. The calculations are thus performed through finite element calculations, using the ZeBuLoN code,[40] with the same assumptions as those of the analytical calculations. The results are presented in Fig. 4c–f. In the case of a ZrO_2 phase not completely embedded in the Al_2O_3 phase (Fig. 2b–d, Fig. 4a, c and e), the value of the normal stress (σ_y) at the interface is lower at points A and C (Fig. 4e) than in the axi-symmetrical case. These stress levels are however sufficiently high to explain crack propagation along these interfaces (Fig. 2b–d). In the case of an elongated ZrO_2 phase (Fig. 2e, Fig. 4b, d and f), the level of the normal stress (σ_y) at point A is high (Fig. 4f), which explains crack propagation along this interface (Fig. 2e). It should be noted that this normal stress is higher than in the axi-symmetrical case, whereas the normal stress (σ_x) at point B (Fig. 4d) is lower than the normal stress in the axi-symmetrical case. The normal stress (σ_y) at point C inside the elongated phase is also very high (Fig. 4f), which explains the crack propagation across this phase (Fig. 2e).

As compared to the ultimate tensile strength of such eutectic ceramics,[2,13] the level of these internal stress components is very high, which, added to the applied loading, explains their essential role in crack nucleation and propagation. Moreover, determination of the normal stress (and, near the surface, of the shear stress) acting on the interfaces explains the possibility of crack deflection in the interfaces in the ternary eutectic ceramics, a phenomenon which may markedly improve the toughness of these DSE ceramics.

The level of the internal stresses found in the alumina phase of the ternary eutectic composites using fluorescence piezospectroscopic internal stress measurements (Table 3) may be compared to the results found using either the concentric cylinder model (Fig. 3) or the more representative models (Fig. 4). In this context, it should be noted that even if a complete description most probably involves a combination of both the "bulk representative" hydrostatic model and of the "surface representative" planar isotropic model, the level of the (σ_{planar}) internal stress in the alumina phase of the ternary Al_2O_3/GAP/ZrO_2 eutectic composite is in good agreement with the calculated thermal mismatch stresses, the alumina phase being under a high level compressive loading for the three stress components: σ_r, σ_θ and σ_z.[9] From a mechanical viewpoint, the hypothesis of a "surface representative" planar isotropic model, leading to the (σ_{planar}) internal stress, may be justified through a FE calculation of the variation of the stress component σ_z near the surface. Assuming that the laser beam is focused on a large cylindrical Al_2O_3 phase, 4 μm in diameter, surrounded by a thin (0.5 μm) ZrO_2 layer (Fig. 5a), the variation of σ_z, as a function of depth along the z axis, is given in Fig. 5b. At a depth of 1 μm, the stress component σ_z is negligible as compared to its maximum value, whereas at a depth of 2 μm, it only attains half its maximum value. Consequently, the real value of the internal stress level is probably comprised between those given by the "bulk representative" hydrostatic model and the more "surface representative" planar isotropic model.

As mentioned earlier, in the present investigation, the observation of crack propagation is performed on the polished and tensile-subjected surface of the specimen. In this context, does the presence of the neighbouring surface exert so strong an influence on crack branching, as it does on interface debonding through the thermal mismatch stress component τ_{rz}? First of all, it should be noted that crack branching is observed not only in the interfaces where crack deflection through debonding has occurred,[9] but also in an individual phase (Fig. 2a). In this last case, the bifurcation mechanism is most probably related to the presence of an underlying phase of the 3-D interconnected microstructure, hidden under the surface. When the macroscopic crack attains this hidden phase, bifurcation may occur through interface debonding on this phase. In this context, it should be noted that bifurcation mechanism generally leads to stopped cracks. Although performed on the specimen surface, the observation of crack branching, which has a non-negligible role in energy dissipation, may be supposed to be representative of the behaviour of the bulk material.

4.2. Stress distribution resulting from an applied loading

As mentioned earlier, in the ternary eutectics, the internal mismatch stresses are sufficiently high to explain the crack propagation modes, especially the deflection of cracks in the interfaces. However, in the binary eutectics, the propagation modes are similar, whereas the internal stresses are much lower and can only help the nucleation and propagation of cracks. In this context, another specific aspect of the eutectic ceramics has to be taken into consideration: the non-uniform stress distribution in such two-phase or three-phase specimens subjected to a uniaxial applied loading. As a matter of fact, the eutectic ceramics differ from a one-phase single crystal by two factors: the 3-D interconnected microstructure and the ratio between the Young's moduli of the various phases, which is different from 1. These two factors involve a non-uniform stress distribution. This phenomenon was revealed through a paradoxical observation. Basal slip was identified in the alumina phase of

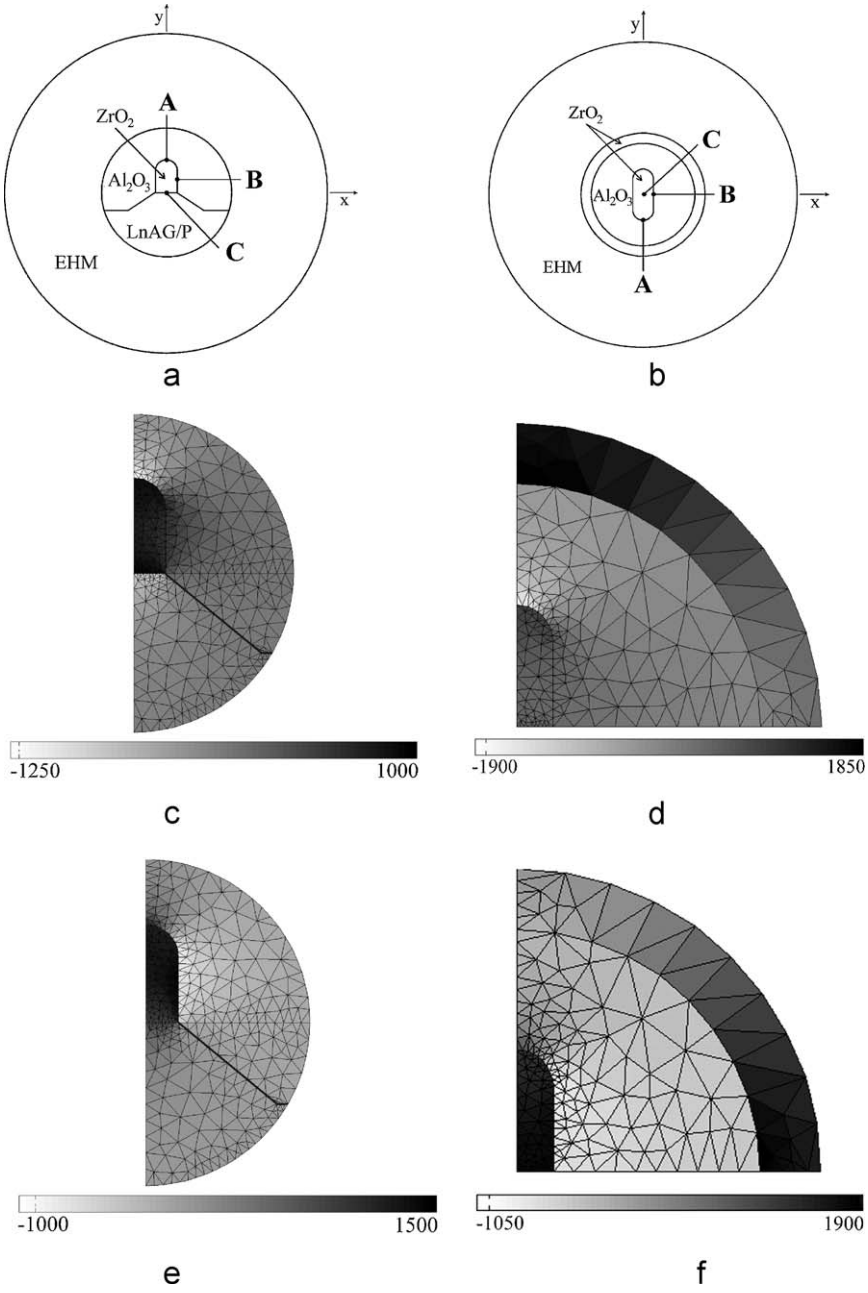

Fig. 4. FE stress calculations in geometrical configurations too complex for a concentric cylinders model to apply. A situation representative of a ZrO_2 phase not completely surrounded by Al_2O_3 (e.g. Fig. 2b (center), c (center) and d (bottom)) is given in (a), whereas the model of an elongated ZrO_2 phase (e.g. Fig. 2e (center)), is given in (b). The σ_x and σ_y stress components corresponding to configurations (a) and (b) are given by grey level density maps (unit: MPa); σ_x in (c) and (d), and σ_y in (e) and (f).

an Al_2O_3/GAP eutectic[8] previously subjected to a compressive creep test (Fig. 6a). This is in agreement with the fact that the basal slip system has the lowest critical resolved shear stress at high temperature.[41,42] However, due to the crystallographic orientation of the compressive creep test specimens, the basal plane is oriented parallel to the loading direction and the shear stress on the basal planes would be negligible in a one-phase single crystal. The only slip system which could be activated would be the prismatic slip system. Thus, the fact that the only observed slip system is the basal slip system implies a stress redistribution in the alumina phase.

Concerning the possible role of the Young's modulus ratio in the eutectic ceramics, this ratio, $E_{G\ or\ P}/E_{Al_2O_3}$, is only approximately 0.7 and thus far from the extreme situations of a hole in a plate (ratio = 0), or of a rigid bar inserted in the hole of a plate (infinite ratio). However, FE calculations performed on a representative two-phase model have shown that the shear stress $|\tau|$ in the loading direction (applied loading Σ) may locally attain 0.1 Σ in the alumina phase (Fig. 6b), whereas it would be zero in a one-phase single crystal. As a comparison, the maximum shear stress in a single crystal, in a plane oriented at 45° to the loading axis, is 0.5 Σ· This stress redistribution, resulting from

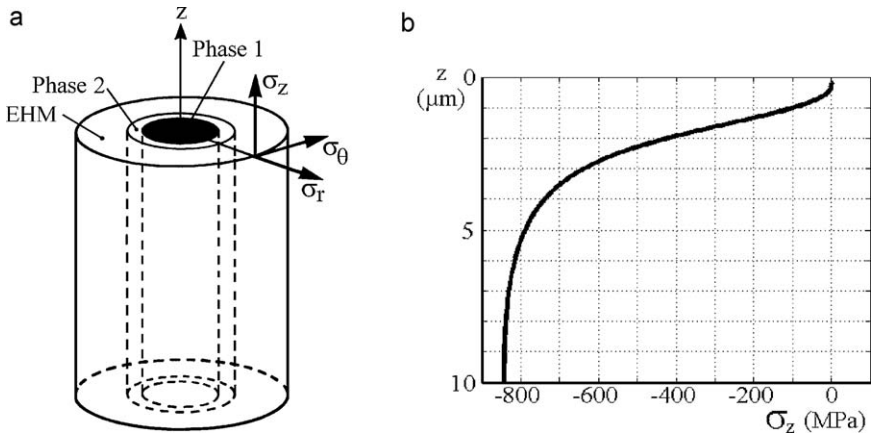

Fig. 5. Hydrostatic and plane stress models in micrometer scale fluorescence piezo-spectroscopy. FE calculation of the variation of the stress component σ_z near the surface, along the z axis, in a large cylindrical Al_2O_3 phase (Phase 1), 4 μm in diameter, surrounded by a thin (0.5 μm) ZrO_2 layer (Phase 2) (a). Variation of σ_z as a function of depth (b).

the Young's modulus ratio of the two-phase eutectic ceramics subjected to a uniaxial loading, is thus strong enough to activate the basal slip system although the direction of the uniaxial loading is parallel to the basal plane. In this respect, it should be noted that the inhomogeneous spatial distribution of the equivalent strain rate in the alumina phase in the plastic region of an Al_2O_3/YAG eutectic has already been evidenced.[43]

As regards the preferential role of curved interfaces in the propagation of cracks, a stress concentration at the interface between the two phases may also result from the ratio between the Young's moduli of the various phases. In the case of a very simple model such as a two-phase plate subjected to a tensile loading (Fig. 6c), the stress concentration factor may be easily determined through analytical formulae.[44–46] Even in the case of such a simple arrangement, the normal stress at the interface at point A (Fig. 6c) is already increased by a factor of ≈1.1, as compared to a one-phase single crystal ($\sigma_r(r=\rho, \theta=0^\circ)=\sigma_n(A)\approx 1.1\ \Sigma$). This local stress concentration may help crack nucleation and propagation, essentially in the binary eutectics where the level and thus the contribution of the thermal mismatch stresses is lower. Consequently, the role of the Young's modulus ratio ($E_{G\ or\ P}/E_{Al_2O_3}$) of the two-phase interconnected microstructure may be considered as essential, not only in the activation of deformation mechanisms, but also in the crack nucleation and propagation modes in the binary eutectics.

4.3. Role of the interfaces

Even if the thermal mismatch stresses and the stress redistribution resulting from an applied loading (for $E_{G\ or\ P}/E_{Al_2O_3} \neq 1$) obviously play a non negligible role in the crack propagation modes, the various mechanisms involved in the nucleation and propagation of cracks have to be considered more precisely. As mentioned earlier, the observed crack propagation modes are: transgranular crack propagation through cleavage, which is a well-known mechanism in ceramics, crack branching, which may be attributed to the 3-D interconnected microstructure and, finally, crack deflection in the interfaces.

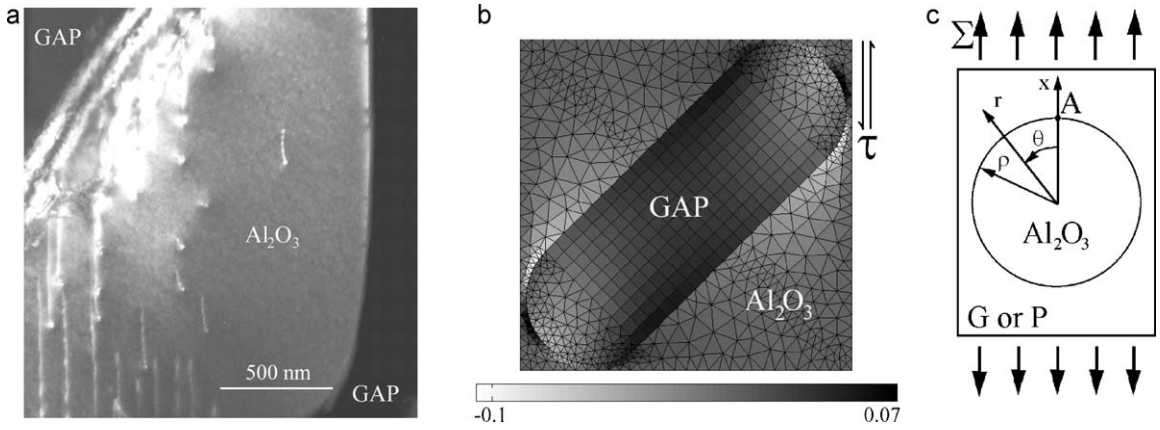

Fig. 6. Stress redistribution in the eutectics subjected to a uniaxial loading ($E_{G\ or\ P}/E_{Al_2O_3} \approx 0.7$). Basal slip in the Al_2O_3 phase of an Al_2O_3/GAP eutectic previously subjected to a compressive creep test with basal plane oriented parallel to the loading direction (a). Representative model and FE calculations of the shear stress τ in a direction parallel to the applied loading (b). Two-phase eutectic specimen: an Al_2O_3 phase embedded in either a garnet (G) or perovskite (P) phase (G or P plate), subjected to a tensile loading (c). Stress concentration factor at point A: $\sigma_r(r=\rho, \theta=0^\circ)=\sigma_n(A)\approx 1.1\ \Sigma$ (c).

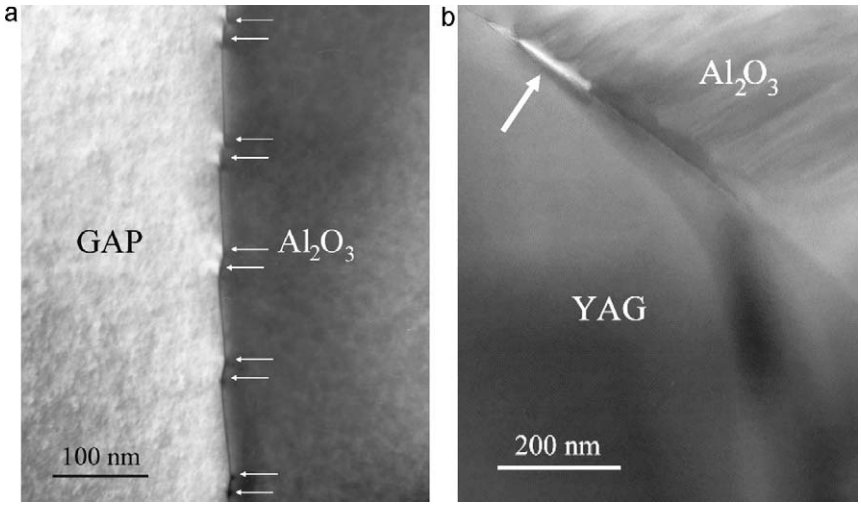

Fig. 7. TEM examination of a curved interface: presence of steps and dislocation pairs at each step (arrows) (a). Crack nucleation (arrow) in an Al_2O_3/YAG interface (b).

In this respect, the specific aspects of the interfaces in the DSEs have to be taken into consideration. First of all, there is no interphase layer, contrary to sintered ceramics. The interfaces are clean, often presenting an intrinsic dislocation network.[1,2,6] However, due to the presence of intrinsic dislocations and possible dangling bonds, the interfaces are weaker than the individual phases. Moreover, curved interfaces are preferential sites of crack deflection.[9] In the case of curved interfaces, transmission electron microscopy examinations have revealed the presence of steps and dislocation pairs (Fig. 7a), thus leading to a further interface weakening. Crack nucleation in the interface between two adjacent phases (Al_2O_3/YAG) has also been observed in TEM (Fig. 7b). Such an observation confirms the weakness of the interfaces as compared to the individual phases and explains the essential role of the interfaces in the nucleation and deflection of cracks.

5. Conclusion

The crack propagation modes observed in directionally solidified eutectic ceramics seem to be drastically influenced by several factors: the thermal mismatch stresses, the stress concentration factors resulting from the Young's modulus ratio of the various phases and the nature of the interfaces.

Concerning the internal stresses, fluorescence piezospectroscopy has allowed an experimental measurement of the internal stresses in the alumina phase of the binary and ternary eutectics. The level of the residual stresses in the alumina phase of the eutectic composites is in good agreement with that found using either a concentric cylinder model or more representative models for the calculation of the thermal mismatch stresses. This stress level, determined through analytical and FE numerical calculations, is sufficiently high to explain the crack propagation modes in the ternary eutectics and to help crack propagation in the binary eutectics. Moreover, the combined effect of the σ_r normal stress and of the τ_{rz} shear stress near the surface, on the possible nucleation of cracks, has been evidenced. In this context, it should be noted that thermal cycling during service of a turbine blade may result in a to and fro displacement of the zirconia phase inside the alumina phase, thus leading to interface damage and finally to debonding. Furthermore, the role of the Young's modulus ratio ($E_{G\,or\,P}/E_{Al_2O_3}$) of the two-phase interconnected microstructure is far from being negligible, not only in the activation of deformation mechanisms, but also in the crack nucleation and propagation modes in the binary eutectics.

The role of the interfaces in the propagation and deflection of cracks seems to be essential. As confirmed through TEM examinations, the interfaces, although clean and strong, are however weaker than the individual phases. Nevertheless, the problem is rather complex and requires a more detailed investigation of the interfaces and especially of the curved interfaces which play an essential role in crack propagation. Moreover, it should be noted that the observed crack deflection modes in the various phases and in the interfaces are more numerous in ternary than in binary eutectics. This experimental result is in good agreement with the previously determined improvement of the fracture toughness of ternary eutectics as compared to binary eutectics.[4,6]

Consequently, due to the presence of a two- or three-phase 3-D interconnected microstructure, a highly detrimental crack propagation mode such as transgranular crack propagation in the brittle ceramic phases is drastically limited by energy dissipative crack deflection modes resulting from thermal mismatch stresses, effects of Young's modulus ratios and nature of the curved interfaces between the various phases.

Finally, this better knowledge of the mechanical behaviour of DSE ceramics has led to the development of a specific Bridgman furnace (Cyberstar, Grenoble, France) according to the specifications established by Onera. This device, which includes two superposed radiofrequency heating elements, is specifically designed to produce large eutectic crystals (up to 50 mm in diameter and 200 mm in height) and turbine blades. In this context, new eutectic compositions without Al_2O_3 phase are under investigation to improve the resistance of the DSE composites to high temperature water vapor corrosion.

Acknowledgements

The authors would like to thank M.-H. Ritti (dilatometric measurements), A. Mavel (compression tests), M. Raffestin (FEG-SEM investigation), K. Makaoui (fluorescence piezospectroscopy measurements), Drs. O. Lavigne, P. Beauchêne and C. Huchette for their kind cooperation and fruitful discussions.

References

1. Waku Y, Nakagawa N, Wakamoto T, Ohtsubo H, Shimizu K, Kohtoku Y. A ductile ceramic eutectic composite with high strength at 1873 K. *Nature* 1997;**389**:49–52.
2. Waku Y, Nakagawa N, Wakamoto T, Ohtsubo H, Shimizu K, Kohtoku Y. High temperature strength and stability of unidirectionally solidified Al_2O_3/YAG eutectic composite. *J Mater Sci* 1998;**33**:1217–25.
3. Llorca J, Orera VM. Directionally solidified eutectic ceramic oxides. *Prog Mater Sci* 2006;**51**:711–809.
4. Piquet N. Microstructures interconnectées dans des eutectiques à base d'oxydes réfractaires élaborés par solidification dirigée. Doctorate thesis, Univ. Paris XII; 2006.
5. Perrière L. Elaboration par solidification dirigée et comportement mécanique de céramiques eutectiques à base d'oxydes réfractaires. Rôle de la microstructure sur la fissuration et la déformation plastique à haute température. Doctorate thesis, Univ. Paris-Est; 2008.
6. Mazerolles L, Piquet N, Trichet MF, Parlier M. Microstructures and interfaces in melt-growth Al_2O_3–Ln_2O_3 based eutectic composites. *Adv Sci Technol* 2006;**45**:1377–84.
7. Mazerolles L, Piquet N, Trichet MF, Perrière L, Boivin D, Parlier M. New microstructures in ceramic materials from the melt for high temperature applications. *Aerospace Sci Technol* 2008;**12**:499–505.
8. Mazerolles L, Perrière L, Lartigue-Korinek S, Piquet N, Parlier M. Microstructures, crystallography of interfaces and creep behavior of melt-growth composites. *J Eur Ceram Soc* 2008;**28**:2301–8.
9. Perrière L, Valle R, Mazerolles L, Parlier M. Crack propagation in directionally solidified eutectic ceramics. *J Eur Ceram Soc* 2008;**28**: 2337–43.
10. Dickey EC, Frazer CS, Watkins TR, Hubbard CR. Residual stresses in high temperature ceramic eutectics. *J Eur Ceram Soc* 1999;**19**: 2503–9.
11. Suzuki H, Akita K, Yoshioka Y, Waku Y, Misawa H. Evaluation of phase stresses of Al_2O_3/YAG binary MGC by synchrotron radiation – residual stress states and stress behavior of YAG phase. *J Soc Mater Sci Jpn* 2003;**52**:770–5.
12. Torii S, Kamiyama T, Oikawa K, Waku Y, Fukunaga T. Strain measurement of the directionally solidified eutectic $Al_2O_3/Y_3Al_5O_{12}$ (YAG) ceramic by neutron diffraction. *J Eur Ceram Soc* 2005;**25**:1307–11.
13. Peña JI, Larson M, Merino RI, de Francisco I, Orera VM, Llorca J, Pastor JY, Martín A, Segurado J. Processing, microstructure and mechanical properties of directionally-solidified Al_2O_3–$Y_3Al_5O_{12}$–ZrO_2 ternary eutectics. *J Eur Ceram Soc* 2006;**26**:3113–21.
14. Gouadec G, Colomban P, Piquet N, Trichet MF, Mazerolles L. Raman/Cr^{3+} fluorescence mapping of a melt-grown $Al_2O_3/GdAlO_3$ eutectic. *J Eur Ceram Soc* 2005;**25**:1447–53.
15. Orera VM, Cemborain R, Merino RI, Peña JI, Larrea A. Piezo-spectroscopy at low temperatures: residual stresses in Al_2O_3–ZrO_2 (Y_2O_3) eutectics measured from 77 to 350 K. *Acta Mater* 2002;**50**:4677–86.
16. Adams JW, Nakamura HH, Ingel RP, Rice RW. Thermal expansion behavior of single-crystal zirconia. *J Am Ceram Soc* 1985;**68**:C228–31.
17. Tsukuma K, Kubota Y, Nobugai K. Thermal and mechanical properties of Y_2O_3-partially stabilized zirconia. *J Ceram Assoc Jpn* 1984;**92**: 233–7.
18. Terblanche SP. Thermal-expansion coefficients of yttria-stabilized cubic zireonias. *J Appl Crystallogr* 1989;**22**:283–4.
19. Hayashi H, Saitou T, Maruyama N, Inaba H, Kawamura K, Mori M. Thermal expansion coefficient of yttria stabilized zirconia for various yttria contents. *Solid State Ionics* 2005;**176**:613–9.
20. Ingel RP, Lewis III D. Elastic anisotropy in zirconia single-crystals. *J Am Ceram Soc* 1988;**71**:265–71.
21. Goto T, Anderson OL, Ohno I, Yamamoto S. Elastic constants of corundum up to 1825 K. *J Geophys Res* 1989;**94**:7588–602.
22. Gupta TK, Valentich J. Thermal expansion of yttrium aluminium garnet. *J Am Ceram Soc* 1971;**54**:355–6.
23. Alton WJ, Barlow AJ. Temperature dependence of the elastic constants of yttrium aluminium garnet. *J Appl Phys* 1967;**38**:3023–4.
24. Bayer G. Thermal expansion anisotropy of oxide compounds. *Proc Br Ceram Soc* 1973;**22**:39–53.
25. Ochiai S, Ueda T, Sato K, Hojo M, Waku Y, Sakata S, Mitani A, Takahashi T, Nakagawa N. Elastic modulus and coefficient of thermal expansion of Al_2O_3/YAG composite at room to ultra high temperatures. *Mater Sci Res Intern, Spec Technol Publ* 2001;**2**:281–5.
26. Levin EM, McMurdie HF. *Phase diagrams for ceramists (1975 Supplement)*. Columbus, Ohio: The American Ceramic Society; 1975. p. 131–132.
27. Mizuno M. Phase diagrams of the systems Al_2O_3–Ho_2O_3 and Al_2O_3–Er_2O_3 at high temperatures. *Yogyo Kyokai Shi* 1979;**87**:405–12.
28. Mizuno M, Yamada T, Noguchi T. Phase diagrams of the systems Al_2O_3–Eu_2O_3 and Al_2O_3–Gd_2O_3 at high temperatures. *Yogyo Kyokai Shi* 1977;**85**:543–8.
29. Lakiza SM, Lopato LM. Stable and metastable phase relations in the system alumina-zirconia yttria. *J Am Ceram Soc* 1997;**80**:893–902.
30. Waku Y, Sakata S, Mitani A, Shimizu K. High-temperature strength and microstructure of an $Al_2O_3/Er_3Al_5O_{12}/ZrO_2$ ternary MGC. *J Jpn Inst Metals* 2000;**64**:1263–8.
31. Vitman FF, Bartenev GM, Pukh VP, Tsepkov LP. A method for measuring the strength of sheet glass. *Glass Ceramics (Steklo i Keramika)* 1962;**19**:412–4.
32. Schmitt RW, Blank K, Schönbrunn G. Experimentelle Spannungsanalyse zum Doppelringverfahren. *Sprechsaal* 1983;**116**:397–405.
33. Grabner L. Spectroscopic technique for the measurement of residual stress in sintered Al_2O_3. *J Appl Phys* 1978;**49**:580–3.
34. He J, Clarke DR. Determination of the piezospectroscopic coefficients for chromium-doped sapphire. *J Am Ceram Soc* 1995;**78**:1347–53.
35. Gouadec G, Colomban P. Raman spectroscopy of nanomaterials: How spectra relate to disorder, particle size and mechanical properties. *Prog Crystallogr Growth Charact Mater* 2007;**53**:1–56.
36. Gouadec G, Makaoui K, Perrière L, Colomban Ph, Mazerolles L. Polarized micro-Raman study of Al_2O_3–based directionally solidified oxide eutectics containing $GdAlO_3$ perovskite, $Er_3Al_5O_{12}$ garnet and cubic ZrO_2. *J Raman Spectr* 2010;**14**:969–77.
37. Gouadec G, Makaoui K, Perrière L, Colomban Ph, Mazerolles L. Ruby (Cr^{3+}) piezospectroscopy in $GdAlO_3/Al_2O_3(ZrO_2)$, $Er_3Al_5O_{12}/Al_2O_3$ and $Y_3Al_5O_{12}/Al_2O_3(ZrO_2)$ directionally solidified eutectics: comparison between hydrostatic and planar isotropic stress models; submitted for publication.
38. Kurz W, Fisher DJ. *Fundamentals of solidification*. 3rd ed. Trans Tech Publications; 1989.
39. Brunet A, Valle R, Vassel A. Intermetallic TiAl-based matrix composites: investigation of the chemical and mechanical compatibility of a protective coating adapted to an alumina fibre. *Acta Mater* 2000;**48**:4763–74.
40. ZéBuLoN. *ZéBuLoN user's manual*. Published by Ecole des Mines de Paris; 2008.
41. Castillo Rodríguez M, Castaing J, Muñoz A, Veyssière P, Domínguez Rodríguez A. Analysis of a kink pair model applied to a Peierls mechanism in basal and prism plane slips in sapphire (α-Al_2O_3) deformed between 200 °C and 1800 °C. *J Am Ceram Soc* 2008;**91**:1612–7.
42. Castaing J, Munoz A, Gomez Garcia D, Dominguez Rodriguez A. Basal slip in sapphire (α-Al_2O_3). *Mater Sci Eng A* 1997;**233**:121–5.
43. Ochiai S, Sakai Y, Kuhara K, Iwamoto S, Sha J, Okuda H, Tanaka M, Hojo M, Waku Y, Nakagawa N, Sakata S-I, Mitani A, Sato M, Ishikawa T. Analytical modeling of stress-strain behavior at 1873 K of alumina/YAG composite compressed parallel and perpendicular to the solidification direction. *Comp Sci Technol* 2007;**67**:270–7.

44. Muskhelishvili NI. *Some basic problems of the mathematical theory of elasticity*. Groningen: Noordhoff; 1953. p. 212–216.
45. Savin GN. *Stress concentrations around holes*. Oxford: Pergamon Press; 1961. p. 234–265.
46. Lesne P-M, Allio N, Valle R. Combined effects of the fibre distribution and of the fibre-matrix or interphase-matrix transverse ratio on the possible fracture modes of unidirectional composites submitted to a transverse loading. *Acta Metall Mater* 1995;**43**:4247–66.